PCCP

PAPER

View Article Online
View Journal | View Issue

Cite this: *Phys. Chem. Chem. Phys.*, 2025, **27**, 19006

Structural characterization of cyclodextrin and maltodextrin alkali-metal coordination *via* ion mobility-mass spectrometry and computational modeling

Hawkins S. Shepard, Emanuel Zlibut, Jody C. May, Benjamin K. Blakley and John A. McLean *

Cyclodextrins (CDs) are macrocyclic oligosaccharides that have the ability to form host–guest inclusion complexes due to their amphiphilic properties, thereby allowing for an increase in the solubility and bioavailability of encapsulated small molecules, such as food constituents and active pharmaceutical ingredients (APIs). While solution-phase properties of CD inclusion complexes have been extensively studied, less is known about the prevailing coordination environment of metal-CD complexes in the absence of bulk solvent. Here, we investigate the gas-phase structural implications of alkali-metal complexation with the three naturally occurring cyclodextrins (αCD, βCD, and γCD) and a suite of linear maltodextrins using structurally-selective ion mobility-mass spectrometry (IM-MS) analysis. For the maltodextrins, the IM-MS analysis revealed an expected linear relationship between the number of monosaccharide units and the measured collision cross section (CCS), however, the CDs exhibited complex size-mass behavior, notably with βCD adopting nearly the same CCS values as the larger γCD, irrespective of the charge carrier. CCS measurements in helium drift gas were obtained on a drift tube IM instrument and used to align to computational modeling outputs which were interpreted for atomistic-level information including bond distances and coordination geometries. Predicted structures for $[CD + Na]^+$ indicate the unusual gas-phase structural behavior of CDs is a consequence of different charge location preferences for αCD and γCD *versus* βCD. Taken together, this work provides a structural context for the underlying metal–host interactions that serve as scaffolds for higher-order CD complexation and supramolecular assemblies.

Received 9th May 2025,
Accepted 9th August 2025

DOI: 10.1039/d5cp01748c

rsc.li/pccp

Introduction

CDs are a class of macrocyclic oligosaccharide rings characterized by a hydrophilic outer surface and a hydrophobic interior cavity. The amphipathic character of CDs is due to the combinatory effect of the hydroxyl groups crowning each opening of the CD, which approximates the shape of a tapered cylinder (a conical frustum), with the hydrogens and glycosidic oxygens lining the cavity.[1–3] Cyclodextrins are classified based on the number of glucopyranoside units comprising their ring, where α-, β-, and γ-cyclodextrin consist of six, seven, and eight glucopyranoside units, respectively. Maltodextrins are the linear oligomeric counterparts of CDs and can adopt a wider range of subunit lengths, as shorter chain oligosaccharides are generally unable to cyclize due to steric hindrance, whereas larger cyclic structures exhibit low stability due to high rates of hydrolysis (Fig. 1).[1] CDs are widely used in many industrial applications due to their unique chemistries, readily forming inclusion complexes with organic guest ligands, including clinically relevant exogenous compounds. Because dextrins are comprised of glucose sub-units linked with α-1,4 glycosidic bonds which are readily-hydrolyzed by human enzymes, cyclo- and maltodextrins and their decomposition products are generally recognized as safe (GRAS) by the FDA and listed in the US Pharmacopeia.[4] For these reasons, CDs are widely incorporated as excipients in pharmaceuticals to improve the bioavailability of APIs with poor water solubility.[1,5] Frequently, metal species are used to complement CD-API formulations, as the incorporation of a metal cation can further improve solubility.[6,7]

While many studies have demonstrated the use of MS and IM-MS techniques in the characterization of CDs and CD inclusion complexes, far fewer have used such data to elucidate the specific interactions of CDs with metals.[8–14] As noted by Norkus, CD structure, and therefore functionality, is influenced by interactions with metal ions, and since the efficiency of

Department of Chemistry, Center for Innovative Technology, Vanderbilt University, Nashville, TN 37235, USA. E-mail: john.a.mclean@Vanderbilt.Edu

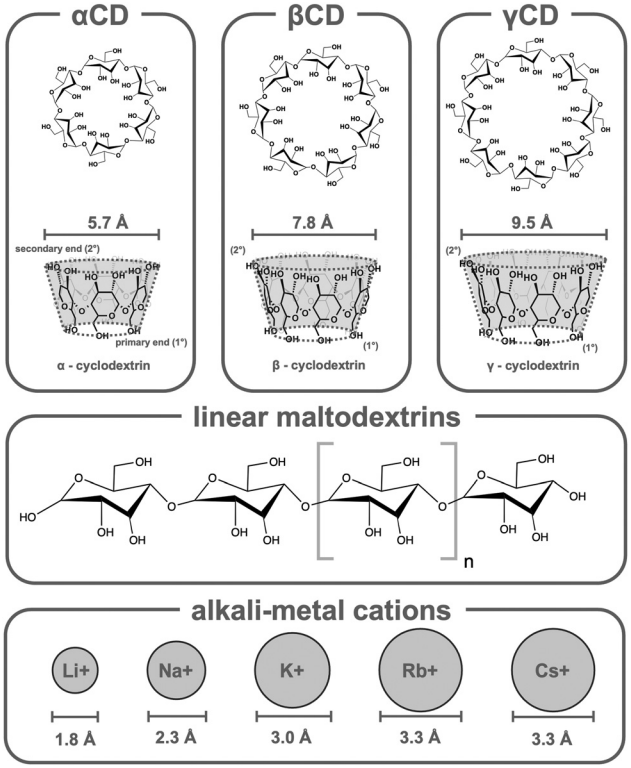

Fig. 1 Structures for α-cyclodextrin (αCD), β-cyclodextrin (βCD), γ-cyclodextrin (γCD), the backbone structure of the linear maltodextrin species analyzed with 4 to 10 glucopyranoside units (n = 1 to 7), and an overview of the alkali-metal cations used for complexation. The diameter of the secondary opening of the cyclodextrins is outlined above the side view structure. The ionic diameters of the alkali-metal cations are displayed below their representations to illustrate the relative length-scales of the different species.

host–guest complex formation is contingent on the structure of the host molecule, understanding the interaction of CDs in the presence of metal ions is important, especially considering the electrolytic composition of biological systems.[15] Studying the conformational behavior of CDs necessitates the use of structurally-selective analytical strategies. Whereas MS offers a highly-sensitive and rapid gas-phase discrimination of ions based on mass-to-charge (m/z), mass measurements alone cannot provide specific information concerning gas-phase conformations.[16–18] However, due to compatible analytical timescales, IM can provide structural insights into the gas-phase behavior of host molecules such as CDs and is often complimented with theoretical modeling.[19–21] Computational investigations can provide predicted gas-phase conformations for host–guest inclusion complexes, including alkali-metal CD complexes to interpret the results obtained in IM-MS experiments.[22] Previous *ab initio* investigations of CD complexes have suggested that metal cations preferentially orient toward the smaller (primary) opening of the CD, favoring the stability afforded by coordinating to the primary hydroxyl groups with reduced steric effects.[23–25] This orientation has become the canonical interpretation of metal-CD complexation, serving as the structural basis for informing subsequent analyses of host–guest incorporation of APIs.[26] However, because initial metal-CD structures hold such an important role in selectivity and guest incorporation, it is imperative to validate the alignment of computational structures with experimental observations.

In this study, we investigate the structural effects of non-covalent alkali-metal coordination to both cyclodextrins and a suite of linear analogs by utilizing a structurally informative MS workflow that integrates highly-accurate drift tube IM measurements with computational modeling. This work investigates the three naturally occurring cyclodextrins—αCD, βCD, and γCD—alongside linear maltodextrins ranging from four to ten glucose units in length, thereby providing a comprehensive analysis of both cyclic and short-chain, linear oligosaccharide systems. Five alkali-metal cations were used to evaluate the impact of ion size, charge density, and coordination preferences on the gas-phase structures of the resulting host–guest complexes. By systematically characterizing the CCS values of these complexes and correlating empirical data with theoretical modeling results, we seek to identify generalizable trends in alkali-metal coordination and to elucidate how these interactions influence the anhydrous structures of metal–dextrin complexes. These findings aim to provide fundamental insights into the non-covalent chemistry of gas-phase carbohydrate complexes and inform the understanding of solution phase host–guest systems for applications ranging from pharmaceutical excipients and food additives to supramolecular assemblies.

Experimental methods

Standards and chemicals

Acetate salts of alkali metals (lithium, sodium, potassium, rubidium, and cesium) as well as high purity (Optima Grade) methanol and water were obtained from Fisher Scientific. Seven linear maltodextrins (maltotetraose, M4; maltopentaose, M5; maltohexaose, M6; maltoheptaose, M7; maltooctaose, M8; maltononaose, M9; and maltodecaose, M10) as well as the three unmodified cyclodextrins (αCD, βCD, γCD) were sourced from MilliporeSigma. All chemicals were used as received.

Sample preparation

All dextrin analyses were performed on mixed cation samples. Initially, 0.01 M stock solutions of each dextrin and alkali acetate salt were prepared in water. An equimolar solution of the five alkali acetates was then prepared in 3 : 2 methanol : water to achieve a total metal cation concentration of 0.01 M. This equimolar mixture of the cations was then combined with the different dextrin stock solutions in a 1 : 1 ratio of cation : dextrin. Finally, sample solutions were serially diluted to a final concentration of 10 μM in 3 : 2 methanol : water for IM-MS analysis.

Ion mobility-mass spectrometry

Each sample was analyzed through direct infusion (10 μL min^{-1}) electrospray ionization (SI, Jet Stream, Agilent Technologies, Santa Clara, CA) coupled to a commercial drift tube IM-quadrupole time-of-flight MS (6560 IM-QTOF, Agilent).[27,28]

The instrument was operated in positive ionization mode and the QTOF was tuned for a mass range of m/z 50-3200. SI source conditions implemented a nitrogen drying gas temperature of 325 °C and a gas flow rate of 5 L min^{-1}, while the ion transfer capillary entrance voltage (V_{Cap}) and the focusing nozzle were set to +3800 V and +2000 V, respectively. All IM measurements were performed using ultra high purity helium drift gas filtered through an inline gas purifier (RMSH, Agilent). IM separations were conducted in a uniform drift field, with a drift tube pressure of ~4 Torr, an ambient temperature of ~300 K, and a drift field of 13.4 V cm^{-1} (drift tube entrance +1272 V; drift tube exit +222 V). IM and QTOF parameters were optimized to maximize the transmission of the non-covalent dextrin-cation complexes. Full settings for IM-QTOF instrumentation are provided in Table S1. Helium drift tube collision cross section ($^{DT}CCS_{He}$) values for the dextrin-cation complexes were determined using the single-field calibration method described by Stow *et al.*[29] Reproducibility of IM measurements was established through interday replicates (n = 6). Reference $^{DT}CCS_{He}$ values for the commercial tuning mixture (ESI-L Tuning Mix, Agilent) used as calibrants were obtained from Morris *et al.*[30] Measured $^{DT}CCS_{He}$ values for cyclodextrins and maltodextrins are presented in Table S2 and S3, respectively.

Computational modeling and theoretical CCS

To provide structural information for the interpretation of experimentally derived $^{DT}CCS_{He}$ values and to estimate dextrin-cation complex coordination geometry, a previously established computational modeling protocol described by Zlibut *et al.* was utilized.[26] This protocol involves both a computational sampling of molecular conformational space and a theoretical calculation of CCS values for computationally generated conformations. Atomic-level structural information, including bond distances and coordination geometries, is attained through evaluation of generated structures that exhibit ±3% alignment with experimental CCS values. Briefly, the computational modeling begins with a Hartree–Fock level geometry optimization implementing a 6-31G* basis set being performed on neutral dextrin molecules in Gaussian 16, with partial charges being derived from *ab initio* electrostatic potential calculations also using a 6-31G* basis set. The restrained electrostatic potential (RESP) program in AMBER was used to fit partial charges, with energy minimization and molecular dynamics simulations also taking place in AMBER. Theoretical CCS measurements were calculated using the projection approximation (PA) in helium implemented in MOBCAL. While more sophisticated CCS prediction algorithms do exist, prior work from our group has compared PA to other algorithms, namely trajectory method and the projected superposition approximation, and results comparing helium-derived CCS values were found to be qualitatively similar. Importantly, PA allows for the generation of a large pool of theoretical structures (*ca.* 3000) using rather modest computational resources, which enables a larger scope of theoretical conformational space to be sampled. We do acknowledge, however, that more sophisticated CCS prediction algorithms may provide increased precision in these structural interpretations. Full details of the computational modeling workflow are provided in the SI (Appendix S1).

Results and discussion

CCS measurements using helium buffer gas

Due to comparatively low polarizability and the predominantly elastic nature of ion–gas collisions, helium is often selected as the drift gas of choice to compare theoretical and experimental IM measurements.[31] In contemporary IM studies, the use of helium is typically replaced by nitrogen due to cost, resistance to electrical breakdown, and increased accessible resolving powers.[32,33] However, because interpretation of computational modeling is dependent upon agreement to empirical CCS measurements, helium drift gas was chosen in this study to complement theoretical CCS conformations generated using the projection approximation parameterized with helium. While CCS values for a particular analyte vary as much as 34% depending on the size and polarizability of the drift gas implemented, previous investigation of chemically-similar dextrin systems has found that $^{DT}CCS_{He}$ determined from experiments conducted in helium correlate closely with measurements performed in nitrogen ($^{DT}CCS_{N2}$).[22,26,32]

The single-field calibration method implemented in this work enables broadband spectral conversion of arrival times to CCS values. In the context of the uniform field drift tube instrumentation used here, single-field CCS calibration strategies are often contrasted by conventional stepped-field methods, wherein the drift field is varied to determine ion mobility from first principles independent of external calibrants. While both approaches to calculating CCS values are effective under appropriate conditions, the single-field calibration method was chosen to mitigate the risk of electrical discharge when using helium drift gas under higher drift fields of the stepped-field method.[30] Since the single-field approach necessitates the use of calibrants with well-characterized CCS values and also relies on empirical regression, the $^{DT}CCS_{He}$ values calculated for the dextrin–cation complexes were validated against an internal standard and compared to previously reported experimental CCS values whenever possible.

The arrival time of the unbound cesium cation (Cs^+, m/z 132.90) was measured concurrent with the primary complexes of interest. Implementing the same calibration curves as were used for the dextrin species, the $^{DT}CCS_{He}$ value of Cs^+ was determined to be 29.05 ± 0.01 $Å^2$ (n = 30), which is within 2% of the value reported by Ellis *et al.* of 29.6 $Å^2$ ± 3%.[34] Additionally, when comparing $^{DT}CCS_{He}$ values, namely $[\alpha CD + Na]^+$ and $[\beta CD + Na]^+$, calculated in this study with values measured on legacy IM platforms, the values are consistent with both the error associated with reproducibility and expected cross-instrument variability.[35] As such, the $^{DT}CCS_{He}$ values presented in this work are considered accurate.

Examining the $^{DT}CCS_{He}$ values determined in this study reveals an expected general increase in size as the number of

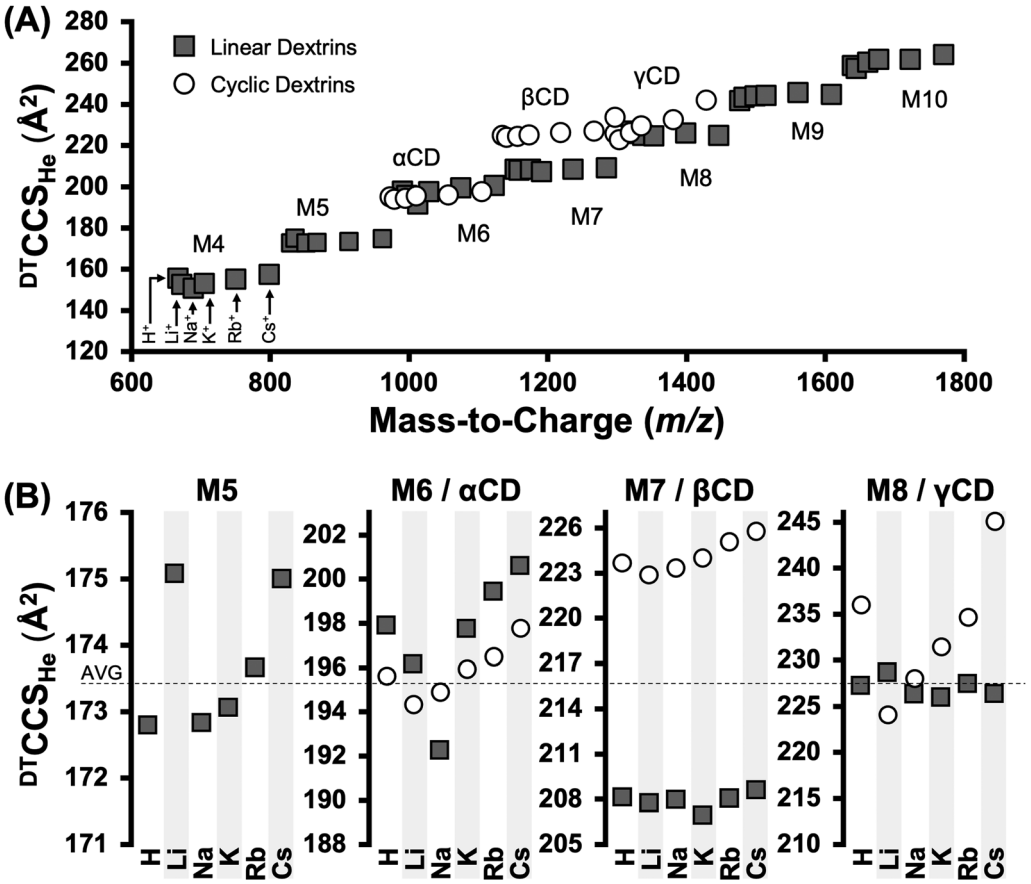

Fig. 2 (A) Conformational space projection (CCS *vs.* *m*/*z*) of measured $^{DT}CCS_{He}$ values for protonated and alkali-metal adducted cyclic and linear dextrin species. Error bars are within the size of each data point (n = 6). (B) CCS plots for maltopentaose (M5) as well as the cyclodextrins and their same-length linear counterparts. Plots are scaled to ±5% of the average (AVG) value to facilitate comparisons.

constituent glucose subunits increases (Fig. 2A). Each of the seven linear dextrins, as well as the three cyclodextrins, were observed to form complexes with each of the five alkali cations as well as protonated $[M + H]^+$ adducts. Higher order complexes (*e.g.*, $[M + 2X]^{2+}$, $[2M + X]^+$, Fig. S1) are also observed in the IM-MS spectra which show evidence of broad peak distributions indicative of the presence of multiple, unresolved conformers, though these higher-order complexes are not discussed in this present work. Importantly, there is no evidence for multiple structural isomers coexisting within the IM peak profiles for any of the mononuclear carbohydrate–metal complexes, $[M + X]^+$, that are the focus of this study. Specifically, the mobility distributions of $[\beta CD + K]^+$ and $[\beta CD + Na]^+$ both benchmark at the expected resolution of this instrument (helium gas, $R_p \sim 40$), and thus show no evidence of peak broadening which would otherwise indicate conformational diversity.[30] Furthermore, high-resolution IM (HRIM) analyses of $[\beta CD + Na]^+$ on a TWSLIM platform found no evidence of conformational isomers under high IM resolution analysis (R_p = 167, Fig. S2). Previous studies of βCD-sodium complexes using a multi-pass TWSLIM platform also noted only one primary gas-phase structure.[36] As such, the experimental mononuclear βCD data presented in this work is interpreted in the context of a single, predominant gas-phase structure existing within the IM measurements.

Because the alkali metals were introduced as equimolar mixtures, the relative abundances observed provide insights into the preferred cation affinities of these carbohydrates. Observations are similar for all dextrins, with Na^+ and K^+ adducts exhibiting the highest abundances, whereas the remaining cations (Li^+, Rb^+, and Cs^+) being present in minor relative abundances (20% or less). Sodium complexes exhibited the highest measured abundances for all carbohydrates except αCD and βCD, where both the sodium and potassium adduct showed similarly high abundances. Interestingly, protonated adducts are generally not observed prominently for carbohydrates, however here the $[M + H]^+$ species is observed in high abundance for both αCD and γCD, although it should be noted that no efforts were made to incorporate acid additives or pH modifiers to these samples. Interday abundance comparisons and $^{DT}CCS_{He}$ for each dextrin are summarized in Fig. S3 and S4.

While empirical $^{DT}CCS_{He}$ values generally increase with the ionic radii of the alkali metal cation for CD complexes, several maltodextrin host–ion pairs exhibit deviations from this correlation. While all maltodextrin–metal complexes of the same carbohydrate length display a similar %CCS difference of $< 5\%$,

complexes incorporating the smallest alkali metal cation, $[M + Li]^+$, frequently do not represent the most compact ion form. This non-intuitive size correlation may arise from host–ion specific interactions such as conformational locking or variations in binding preferences and hydrogen bonding networks that directly influence the resulting gas-phase conformations. These effects, though subtle, may reflect metal-dependent intramolecular folding, wherein certain cations are more conducive for initiating structural compaction despite possessing larger ionic radii.

The magnitude of these changes in CCS varies in response to cation binding also appears to correlate with the host size. For example, when comparing the smallest and largest cations in this study, αCD and βCD both exhibit only a modest increase of ~1.8% between Li^+ and Cs^+, whereas γCD demonstrates a much larger 8.7% increase. This larger observed difference in CCS could suggest greater conformational flexibility or variable coordination behavior in γCD, which is consistent with prior observations in cyclic ionophores, where ion coordination geometry and cavity size influence metal binding and structural compaction.[37]

When comparing the same cation across the various maltodextrin complexes, a high degree of linearity with respect to m/z and $^{DT}CCS_{He}$ trends are observed, with all cation-specific mobility-mass (CCS-m/z) correlations exhibiting an R^2 greater than 0.99. A representative plot displaying the linearity of the maltodextrin suite for the sodium complex is found in Fig. 3, with the remaining plots being included in Fig. S5. Conservation of linearity in individual alkali metal trends correlates to adduct type rather than number of dextrin units, indicating that the dominant influence on gas-phase structure for these linear species is the charge carrier. Thus, the unique charge distribution and coordination of the different alkali metal cations are the key drivers of the observed gas-phase conformations as reflected in their corresponding $^{DT}CCS_{He}$ values.

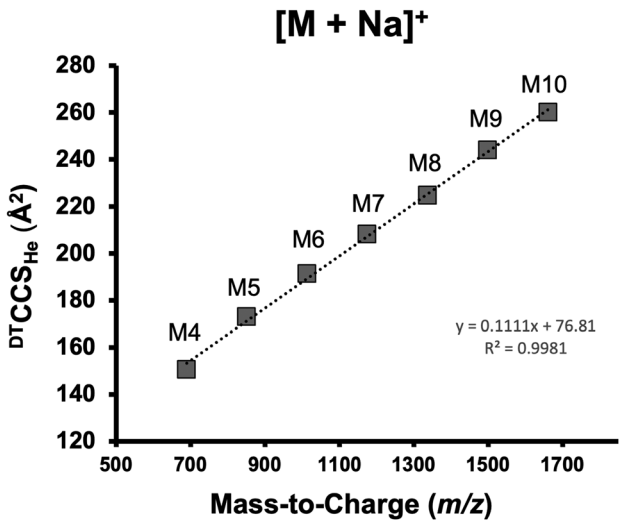

Fig. 3 Representative regression plot displaying linearity of maltodextrin analytes complexed with sodium. All cation-specific mobility-mass correlations exhibit an R^2 greater than 0.99.

Interestingly, a similar linear trend for analytes with the same charge carrier is not observed for the cyclodextrins, suggesting that the contribution of the alkali metal type is likely masked by the gas-phase structure of the corresponding CD-metal complex, as might be expected if the cation were bound within the cavity of the CDs (Fig. S6). The specific CCS differences observed are likely due to the diminished degrees of freedom inherently associated with a cyclic structure, with number of dextrin subunits present within the ring largely dictating the coordination geometries. This difference becomes especially evident when comparing the $^{DT}CCS_{He}$ values of the three cyclodextrins alongside the maltodextrins containing the same number of subunits (Fig. 2B). For example, the sizes of the sodium complexes for M6 compared to αCD (0.63%) as well as M8 compared to γCD (1.33%) are all within 2% of one another. However, the sodium complex of M7 and βCD exhibits a stark difference of 7.48%. Because M7 falls along the empirical trendline for the maltodextrin series, this comparatively large %CCS difference between M7 and βCD is not a consequence of M7, but rather due to the anhydrous structure of βCD exhibiting a size larger than would be predicted from the linear dextrin trend. This apparent anomalous increase in size is observed in all of the metal complexes formed by βCD, including $[\beta CD + H]^+$ suggesting this increase in CCS is specific to the gas-phase structural preference of βCD and not a consequence of specific cation coordination.

Structural insight from computational modeling

To investigate this observation further, sodium-coordinated complexes for M7 and the three cyclodextrins were computationally modeled. Conformational scatter plots for each of the four systems were generated by plotting the theoretically-predicted CCS values of 3000 energy-minimized structures obtained *via* projection approximation parameterized in helium ($^{Theor,PA}CCS_{He}$), against their calculated relative energies (Fig. 4). Distribution frequencies for each calculated dimension (CCS and relative energy) are shown in the adjacent histograms. Experimental $^{DT}CCS_{He}$ values measured for each complex are overlayed with shaded regions corresponding to ±3%. Predicted structures falling within this ±3% window were considered to be in alignment and were prioritized in further hierarchical clustering analysis.

By subjecting candidate structures to a clustering analysis based on the root-mean-square (RMS) distance of atoms from superimposed structures (Table S4), a representative candidate structure for the gas-phase conformations of each complex can be visualized. These average structures were selected based on their RMS deviation from the mean and provide a visual reference (Fig. 4) for the molecular geometry of the sodium-coordinated complexes. The side views provide a lateral perspective that distinguishes both secondary and primary hydroxyls, while the bottom view represents a perspective of looking through the primary opening of the conical frustum.

The differences in the relative location of the sodium cation in $[\beta CD + Na]^+$ are immediately apparent when compared to the other complexes. Specifically, in $[\alpha CD + Na]^+$, $[M7 + Na]^+$, and

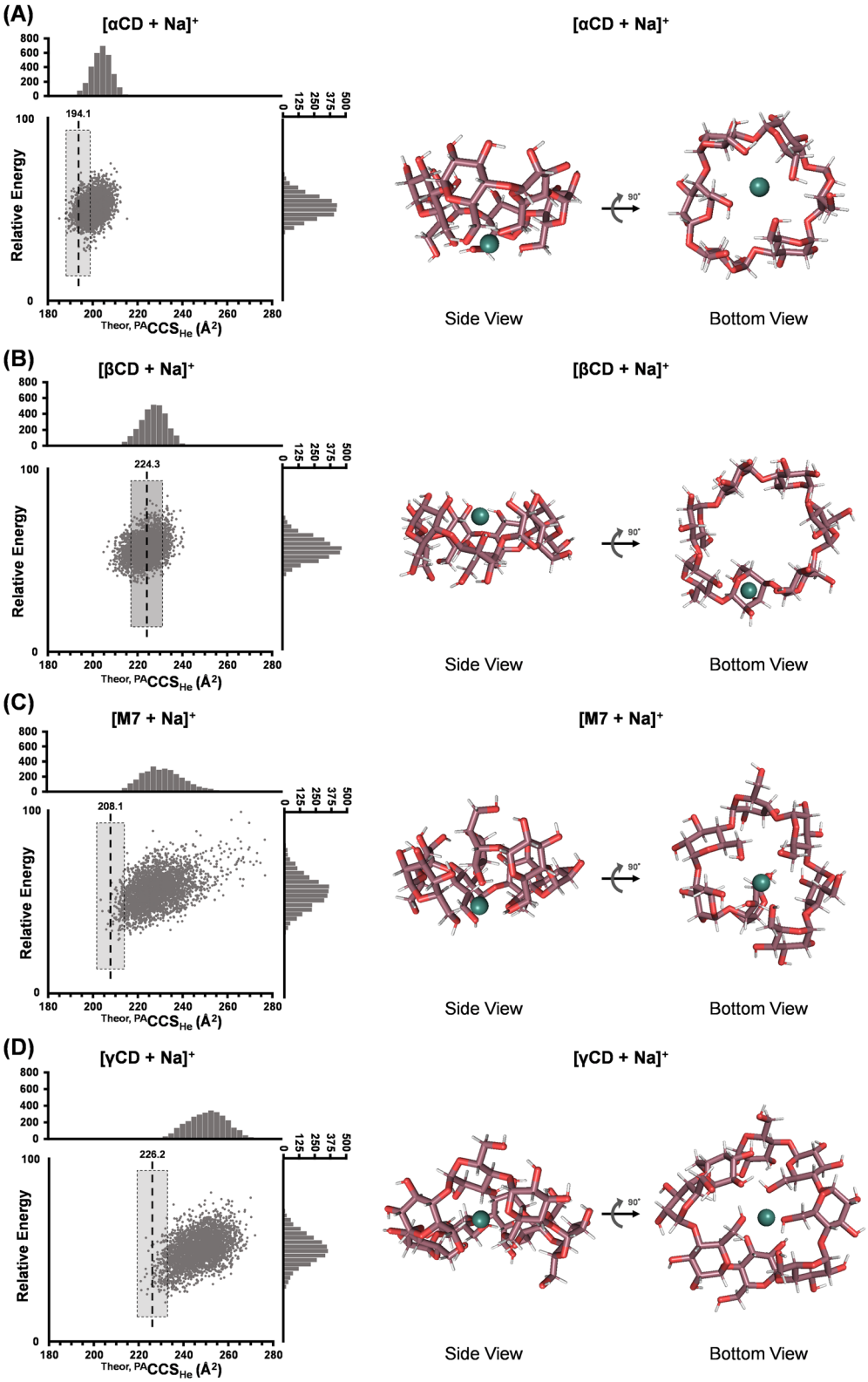

Fig. 4 Theoretical conformational space plots and representative candidate structures for non-covalent complexation of (A) [αCD + Na]$^+$, (B) [βCD + Na]$^+$, (C) [M7 + Na]$^+$, and (D) [γCD + Na]$^+$. Histogram distributions of CCS values (bin size = 2.5 Å^2) and relative energies (bin size = 2.5 kcal mol^{-1}) of theoretical structures are oriented along the corresponding axes. The histogram *y*-axes correspond to the total number of structures. The measured drift tube CCS value for each of the complexes is represented by the vertical dotted line, with the shaded regions representing a threshold corresponding to ±3% of the empirically-measured CCS. Visual representations of candidate structure include a side view (smaller, primary hydroxyl ring on bottom) and a bottom view (looking through the primary opening of the CD). The sodium cation (green sphere) is visually scaled to the same diameter in each projection.

$[\gamma CD + Na]^+$, the sodium cation is incorporated in a central position relative to the carbohydrate subunits and preferentially coordinates with the primary hydroxyls, which is in agreement with previous investigations of site-specific CD complexation, especially those involving $[\alpha CD + Na]^+$.[24] By contrast, the sodium cation present in the average structure of $[\beta CD + Na]^+$ is located along the periphery of the larger, secondary opening of the cyclodextrin.

In the absence of a cation, the structures adopted by cyclodextrins are dictated by the capacity of their secondary hydroxyl groups to interact with and form hydrogen bonds with adjacent moieties. In βCD, all constituent secondary hydroxyls are able to hydrogen bond, allowing for the formation of a symmetrically coordinated ring of hydroxyls along the larger secondary opening of the conical frustum. However, in the cases of αCD and γCD, symmetric coordination of hydroxyls are absent due to the slightly distorted sterics of glucopyranoside units in the former and the non-coplanar, flexible structure of the latter.[1] The linear dextrin M7, despite exhibiting an ouroboric structure, is similarly hindered from adopting an ordered coordination structure due the steric interference resulting from its terminal units not being covalently linked as they are in βCD. The presence of a preorganized network of intramolecular hydrogen bonds in βCD thus provides a thermodynamically-favorable environment for initial metal coordination along the secondary rim of the cyclic structure in solution, which appears to be preserved in the gas phase.[1,38] In the other structures, where this chain of hydrogen bonding is either disrupted or incomplete, the more favorable region for coordination is found to be the center of the smaller, primary opening, where the metal has the greatest probability of interacting with the largest number of primary hydroxyls.

Previous computational studies on metal-CD complexes report two general groups of conformations: those that conserve the initial truncated cone orientation formed by the glucopyranoside residues and those that disrupt this orientation.[25] In this present study, introducing an alkali metal cation to βCD has the effect of disrupting concerted hydrogen bonding, causing the cyclodextrin to distort, with its primary hydroxyls no longer directed inward but instead displaying a more vertical orientation relative to the primary axis of the cavity. This change in structure in response to metal coordination, along with the disruption of hydrogen bonding, results in a measurable increase in the $^{DT}CCS_{He}$ values adopted in the gas phase for $[\beta CD + Na]^+$, likely resulting in the comparatively large %CCS difference between $[\beta CD + Na]^+$ and its linear analog, $[M7 + Na]^+$. Some additional metal-independent structural details are also reflected in the representative candidate structures projected. For example, in the bottom view of $[\alpha CD + Na]^+$, one of the six subunits is visibly canted, underscoring the expectation of distorted sterics associated with αCD. In the context of metal-coordination, however, this has the effect of providing an additional primary hydroxyl capable of coordinating with the sodium cation. Another example is the flexing and flattening of the truncated cone structure observed for $[\gamma CD + Na]^+$, wherein the conical conformation begins to

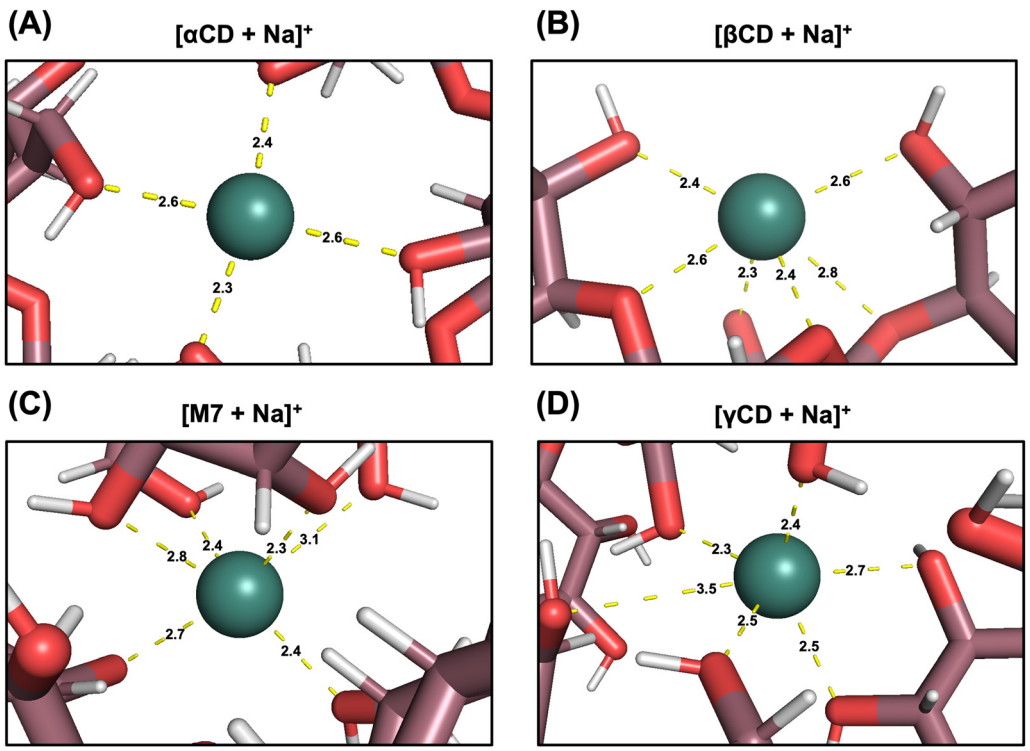

Fig. 5 Coordination environment for (A) $[\alpha CD + Na]^+$, (B) $[\beta CD + Na]^+$, (C) $[M7 + Na]^+$, and (D) $[\gamma CD + Na]^+$. Coordination sphere of sodium (green sphere) was evaluated within a radius of 3.5 Å from the center. Coordinating oxygens indicated by yellow dashed lines representing bond distances measured in Å.

contort into a more disk-like orientation. The asymmetric structural motifs found in the even-numbered cyclodextrin analytes (αCD and γCD) are more likely to mirror the gas-phase structures of their linear counterparts, which would also experience steric differences due to the lack of covalently-bonded terminal glucopyranosides.

A detailed evaluation of the representative candidate structures reveals specific differences in the coordination environment adopted by non-covalent metal–dextrin complexes (Fig. 5). The extent of sodium cation coordination observed in each of the four candidate structures was assessed by analyzing the spatial arrangement and proximity of oxygen atoms within a 3.5 Å radius threshold which was chosen based on reported bond distances associated with alkali-metal coordination.[39] When considering both the total number of interactions and the identities of participating oxygen species, αCD exhibited the most limited coordination sphere, with only four oxygen atoms contributing short-range interactions and each constituent oxygen belonging to a primary hydroxyl (Fig. 5A). By contrast, βCD, γCD, and M7 all demonstrated a more populated coordination environment, with six instances of sodium–oxygen interactions occurring within a distance of 3.5 Å from the metal. Despite containing the same number of interactions, however, the specific oxygens involved in coordination varied widely across the different dextrins. For example, M7 exhibited coordination with five primary hydroxyls and one secondary, terminal hydroxyl due to its linear structure (Fig. 5C). The flattened structure adopted by γCD results in a total of six interactions within 3.5 Å, with an even number (3/3) distributed between primary and secondary hydroxyls (Fig. 5D). To accommodate this higher level of coordination, one glucopyranoside subunit of γCD rotates relative to the others (Fig. S7). Despite the torsion required to adopt this configuration, this candidate structure corresponds to the lowest energy region of the scatter plot, and thus the energy expenditure to contort the subunit may be offset by the additional coordination gained from this configuration.

In terms of interaction distances, the primary hydroxyls of γCD are, on average, closer to the sodium cation, and as such likely exert a stronger influence on the stability and molecular framework of $[\gamma CD + Na]^+$. Finally, for $[\beta CD + Na]^+$, the coordination environment of the representative structure is significantly different than what is predicted for the other three complexes. Due to the favorability of the stabilized hydrogen bonding network along the secondary opening, the candidate $[\beta CD + Na]^+$ configuration is entirely absent of close interactions with any primary hydroxyl oxygens. Instead, the coordinating atoms consist of six constituents, three secondary hydroxyl and three glycosidic oxygens, of which two are oxygens involved in the 1–4 covalent bridge between glucose subunits. The favorable coordination structure which forms along the wider, secondary opening of βCD is likely one of the driving forces dictating the strong host–guest interactions that are characteristic of βCD-based inclusion complexes, and may provide insight into the potential structural perturbations impacting the loading and release of exogenous guest compounds.[22,26] A summary of bond distances for sodium coordination are provided in Table S5, while complete atom list and coordination environments for αCD, βCD, γCD, and M7 can be found in Tables S6, S7, S8, and S9, respectively.

While gas-phase conformations are not expected to be identical to those present in solution, binding preferences resulting from structural properties and intrinsic interactions (namely hydrogen bonding) are able to exist in the gas-phase uninhibited by solvent effects, meaning that gas-phase analyses are representative of preferential binding sites and intrinsic stabilities that serve as the foundation for solution-phase interactions. Furthermore, previous IM-MS and MS/MS studies indicate structural similarity between anhydrous, gas-phase structures and their solution-phase counterparts, thus IM-MS investigations supported by computational modeling can serve as a means to investigate native-like conformations.[40,41]

Conclusions

In this study, we utilize an experimental IM-MS workflow complemented by computational modeling to garner structural information that aids in our understanding of CD inclusion complexes and the specific role of alkali-metal coordination on promoting CD host–guest complexation. Conformational space mapping of the mobility-mass correlations observed in the IM-MS data revealed a highly linear progression of CCS in response to increasing oligomer size of the linear maltodextrins, but also a comparatively anomalous structural ordering of the cyclic dextrins that suggested the CDs adopt unique gas-phase structures. βCD in particular exhibited a strong deviation to larger CCS values relative to the mobility-mass correlations observed in other CDs.

Computational results yielded theoretically generated structures for the coordination complexes. While the HF/6-31G* level of theory has known limitations, particularly in capturing dispersion interactions and precise coordination geometries, the trends observed here are consistent with previously reported DFT-calculated structures, with these results providing a reasonable qualitative model for interpreting gas-phase IM-MS data. Structural interpretation of the aligned candidate structures suggested that all of the dextrins tended to adopt anhydrous structures where the metal ion is positioned symmetrically at the center of the coordination complex, except βCD, which prefers an asymmetric coordination of the sodium towards the secondary hydroxyls of the CD structure. This periphery binding of the metal cation in βCD results in a vacancy that provides a favorable coordination environment for guest inclusion; thus, the metal-coordinated βCD complex adopts a rigid anhydrous structure with a corresponding higher CCS than is observed by the other CDs which may correlate with βCD's high affinity for forming small molecule host–guest complexes.

In the context of pharmaceutical formulation, these results imply that the choice of counterions, excipients, and API can induce specific structural perturbations that could impact drug

loading or release. As IM-MS instrumentation and molecular modeling strategies continue to progress, further examination of metal-CD systems with expansion to multi-charged and non-alkali metal cations and anions, as well as functionalized CDs, will remain integral to the informed application of CD host–guest inclusion complexes.

Author contributions

The manuscript was written collaboratively by all authors, all of whom have approved of the final version of this manuscript.

Conflicts of interest

There are no conflicts to declare.

Data availability

The data supporting the article has been included as part of the SI.

The SI includes IM-MS instrument settings, $^{DT}CCS_{He}$ measurements for cyclodextrin and maltodextrin molecules, an outline of the computational modeling workflow, an RMS clustering analysis of predicted structures, abundance comparisons for cyclodextrin and maltodextrin molecules, individual cation-specific correlations, alternate perspectives of the $[\gamma CD + Na]^+$, summary of bond distances for sodium coordination, and complete atom lists and coordination environments for modeled structures. Initial visualization and processing of empirical data was performed in MassHunter IM-MS Browser 10.0 (Agilent Technologies). Determination of helium CCS values was conducted in Microsoft Excel using the single-field calibration equation and tune mix calibrant helium reference values.[29,30] Theoretical modeling was performed using Gaussian 16 (M. Frisch *et al.*, *Gaussian 16*; Gaussian, Inc.: Wallingford, CT, 2016), AMBER (D. Case *et al.*, Amber 2022; University of California: San Francisco, 2022), and MOBCAL (T. Wyttenbach *et al.* *J. Am. Soc. Mass Spectrom.* 1997, **8**, 275–282). CCS values reported in SI are also deposited and freely-available in the Unified CCS Compendium (J. Picache *et al.*, *Chem. Sci.* 2019, **10**(4), 983–993; **https://mcleanresearchgroup.shinyapps.io/CCS-Compendium/**). See DOI: **https://doi.org/10.1039/d5cp01748c**

Acknowledgements

This work was supported in part using the resources of the Center for Innovative Technology at Vanderbilt University.

Notes and references

1 J. Szejtli, Introduction and General Overview of Cyclodextrin Chemistry, *Chem. Rev.*, 1998, **98**, 1743–1753.
2 T. Kovacs, P. Nagy, G. Panyi, L. Szente, Z. Varga and F. Zakany, Cyclodextrins: Only Pharmaceutical Excipients or Full-Fledged Drug Candidates?, *Pharmaceutics*, 2022, **14**, 2559.
3 L. Szente and J. Szemán, Cyclodextrins in analytical chemistry: Host-guest type molecular recognition, *Anal. Chem.*, 2013, **85**, 8024–8030.
4 K. Uekama, F. Hirayama and T. Irie, Cyclodextrin Drug Carrier Systems, *Chem. Rev.*, 1998, **98**, 2045–2076.
5 S. S. Braga, Cyclodextrins: Emerging Medicines of the New Millennium, *Biomolecules*, 2019, **9**, 801.
6 S. V. Kurkov and T. Loftsson Cyclodextrins, *Int. J. Pharm.*, 2013, **453**, 167–180.
7 Z. He, Z. Wang, H. Zhang, X. Pan, W. Su, D. Liang and C. Wu, Doxycycline and hydroxypropyl-β-cyclodextrin complex in poloxamer thermal sensitive hydrogel for ophthalmic delivery, *Acta Pharm. Sin. B*, 2011, **1**, 254–260.
8 V. Gabelica, N. Galic and E. De Pauw, On the specificity of cyclodextrin complexes detected by electrospray mass spectrometry, *J. Am. Soc. Mass Spectrom.*, 2002, **13**, 946–953.
9 Y. Dotsikas and Y. L. Loukas, Efficient determination and evaluation of model cyclodextrin complex binding constants by electrospray mass spectrometry, *J. Am. Soc. Mass Spectrom.*, 2003, **14**, 1123–1129.
10 M. M. Gaye, R. Kurulugama and D. E. Clemmer, Investigating carbohydrate isomers by IMS-CID-IMS-MS: precursor and fragment ion cross-sections, *Analyst*, 2015, **140**, 6922–6932.
11 Y. Chen, Z. Zuo, X. Dai, P. Xiao, X. Fang, X. Wang, W. Wang and C. F. Ding, Gas-phase complexation of α-/β-cyclodextrin with amino acids studied by ion mobility-mass spectrometry and molecular dynamics simulations, *Talanta*, 2018, **186**, 1–7.
12 V. Bonnet, G. Clodic, C. Sonnendecker, W. Zimmermann and C. Przybylski, Ion mobility mass spectrometry enables the discrimination of positional isomers and the detection of conformers from cyclic oligosaccharides-metals supramolecular complexes, *Carbohydr. Polym.*, 2023, **320**, 121205.
13 C. D. Chouinard, G. Nagy, I. K. Webb, S. V. B. Garimella, E. S. Baker, Y. M. Ibrahim and R. D. Smith, Rapid Ion Mobility Separations of Bile Acid Isomers Using Cyclodextrin Adducts and Structures for Lossless Ion Manipulations, *Anal. Chem.*, 2018, **90**, 11086–11091.
14 Y. Liu and D. E. Clemmer, Characterizing oligosaccharides using injected-ion mobility/mass spectrometry, *Anal. Chem.*, 1997, **69**, 2504–2509.
15 E. Norkus, Metal ion complexes with native cyclodextrins. An overview, *J. Inclusion Phenom. Macrocyclic Chem.*, 2009, **65**, 237–248.
16 B. Baytekin, H. T. Baytekin and C. A. Schalley, Mass spectrometric studies of non-covalent compounds: why supramolecular chemistry in the gas phase?, *Org. Biomol. Chem.*, 2006, **4**, 2825–2841.
17 G. Wadhwa, S. Kumar, L. Chhabra, S. Mahant and R. Rao, Essential oil–cyclodextrin complexes: an updated review, *J. Inclusion Phenom. Macrocyclic Chem.*, 2017, **89**, 39–58.
18 C. A. Schalley, Supramolecular chemistry goes gas phase: the mass spectrometric examination of noncovalent

interactions in host–guest chemistry and molecular recognition, *Int. J. Mass Spectrom.*, 2000, **194**, 11–39.

19 J. C. May and J. A. McLean, Ion mobility-mass spectrometry: Time-dispersive instrumentation, *Anal. Chem.*, 2015, **87**, 1422–1436.

20 J. N. Dodds and E. S. Baker, Ion Mobility Spectrometry: Fundamental Concepts, Instrumentation, Applications, and the Road Ahead, *J. Am. Soc. Mass Spectrom.*, 2019, **30**, 2185–2195.

21 C. Klein, S. M. Cologna, R. T. Kurulugama, P. S. Blank, E. Darland, A. Mordehai, P. S. Backlund and A. L. Yergey, Cyclodextrin and malto-dextrose collision cross sections determined in a drift tube ion mobility mass spectrometer using nitrogen bath gas, *Analyst*, 2018, **143**, 4147–4154.

22 J. C. May, E. Zlibut, B. K. Blakley, C. S. Wood, Y. Wei, B. Showalter, E. Dybeck, E. R. Remish, V. Guidolin, B. A. Bernat and J. A. McLean, Ion Mobility-Mass Spectrometry Strategies to Elucidate the Anhydrous Structure of Noncovalent Guest/Host Complexes, *Anal. Chem.*, 2024, **96**, 2024.

23 S. E. Angelova, V. K. Nikolova and T. M. Dudev, Determinants of the host–guest interactions between α-, β- and γ-cyclodextrins and group IA, IIA and IIIA metal cations: a DFT/PCM study, *Phys. Chem. Chem. Phys.*, 2017, **19**, 15129–15136.

24 F. Gámez, P. Hurtado, A. R. Hortal, B. Martínez-Haya, G. Berden and J. Oomens, Cations in a Molecular Funnel: Vibrational Spectroscopy of Isolated Cyclodextrin Complexes with Alkali Metals, *Chem. Phys. Chem.*, 2013, **14**, 400–407.

25 A. Stachowicz, A. Styrcz, J. Korchowiec, A. Modaressi and M. Rogalski, DFT studies of cation binding by β-cyclodextrin, *Theor. Chem. Acc.*, 2011, **130**, 939–953.

26 E. Zlibut, J. C. May, Y. Wei, D. Gessmann, C. S. Wood, B. A. Bernat, T. E. Pugh, L. Palmer-Jones, R. P. Cosquer, E. Dybeck and J. A. McLean, Noncovalent Host-Guest Complexes of Artemisinin with α-, β-, and γ- Cyclodextrin Examined by Structural Mass Spectrometry Strategies, *Anal. Chem.*, 2023, **95**, 8180–8188.

27 J. C. May, C. R. Goodwin, N. M. Lareau, K. L. Leaptrot, C. B. Morris, R. T. Kurulugama, A. Mordehai, C. Klein, W. Barry, E. Darland, G. Overney, K. Imatani, G. C. Stafford, J. C. Fjeldsted and J. A. McLean, Conformational ordering of biomolecules in the gas phase: Nitrogen collision cross sections measured on a prototype high resolution drift tube ion mobility-mass spectrometer, *Anal. Chem.*, 2014, **86**, 2107–2116.

28 J. C. May, J. N. Dodds, R. T. Kurulugama, G. C. Stafford, J. C. Fjeldsted and J. A. McLean, Broadscale resolving power performance of a high precision uniform field ion mobility-mass spectrometer, *Analyst*, 2015, **140**, 6824–6833.

29 S. M. Stow, T. J. Causon, X. Zheng, R. T. Kurulugama, T. Mairinger, J. C. May, E. E. Rennie, E. S. Baker, R. D. Smith, J. A. McLean, S. Hann and J. C. Fjeldsted, An Interlaboratory Evaluation of Drift Tube Ion Mobility-Mass Spectrometry Collision Cross Section Measurements, *Anal. Chem.*, 2017, **89**, 9048–9055.

30 C. B. Morris, J. C. May, K. L. Leaptrot and J. A. McLean, Evaluating Separation Selectivity and Collision Cross Section Measurement Reproducibility in Helium, Nitrogen, Argon, and Carbon Dioxide Drift Gases for Drift Tube Ion Mobility–Mass Spectrometry, *J. Am. Soc. Mass Spectrom.*, 2019, **30**, 1059–1068.

31 J. C. May, C. B. Morris and J. A. McLean, Ion mobility collision cross section compendium, *Anal. Chem.*, 2017, **89**, 1032–1044.

32 R. T. Kurulugama, E. Darland, F. Kuhlmann, G. Stafford and J. Fjeldsted, Evaluation of drift gas selection in complex sample analyses using a high performance drift tube ion mobility-QTOF mass spectrometer, *Analyst*, 2015, **140**, 6834–6844.

33 J. C. May, E. Jurneczko, S. M. Stow, I. Kratochvil, S. Kalkhof and J. A. McLean, Conformational landscapes of ubiquitin, cytochrome *c*, and myoglobin: Uniform field ion mobility measurements in helium and nitrogen drift gas, *Int. J. Mass Spectrom.*, 2018, **427**, 79–90.

34 H. W. Ellis, E. W. McDaniel, D. L. Albritton, L. A. Viehland, S. L. Lin and E. A. Mason, Transport properties of gaseous ions over a wide energy range. Part II, *At. Data Nucl. Data Tables*, 1978, **22**, 179–217.

35 L. S. Fenn and J. A. McLean, Structural resolution of carbohydrate positional and structural isomers based on gas-phase ion mobility-mass spectrometry, *Phys. Chem. Chem. Phys.*, 2011, **13**, 2196–2205.

36 J. M. Rabus, R. P. Pellegrinelli, A. H. Abi Khodr, B. J. Bythell, T. R. Rizzo and E. Carrascosa, Unravelling the Structures of sodiated β-cyclodextrin and its fragments, *Phys. Chem. Chem. Phys.*, 2021, 13714–13723.

37 E. Nkyaagye, H. J. Olivios and T. D. Do, Ligand Conformational and Metal Coordination Isomers in Complexes of Metal Ions and Cyclic Depsipeptides, *J. Am. Soc. Mass Spectrom.*, 2025, **36**, 873–882.

38 M. E. Davis and M. E. Brewster, Cyclodextrin-based pharmaceutics: past, present and future, *Nat. Rev. Drug Discovery*, 2004, **3**, 1023–1035.

39 O. C. Gagné and F. C. Hawthorne, Bond-length distributions for ions bonded to oxygen: Alkali and alkaline-earth metals, *Acta Crystallogr., Sect. B: Struct. Sci., Cryst. Eng. Mater.*, 2016, **72**, 602–625.

40 H. Lui, G. Yang, Y. Tang, D. Cao, T. Qi, Y. Qi and G. Fan, Physicochemical characterization and pharmacokinetics evaluation of β-caryophyllene/β-cyclodextrin inclusion complex, *Int. J. Pharm.*, 2013, **450**, 304–310.

41 P. Chakraborty, A. Baksi, E. Khatun, A. Nag, A. Ghosh and T. Pradeep, Dissociation of Gas Phase Ions of Atomically Precise Silver Clusters Reflects Their Solution Phase Stability, *J. Phys. Chem. C*, 2017, **121**, 10971–10981.